Pergamon

Parameter ranges in binary solidification from vertical boundaries

GUSTAV AMBERG

Department of Mechanics, Royal Institute of Technology, S-100 44 Stockholm, Sweden

Abstract—Solidification of an alloy by cooling the vertical sides of a rectangular mold is considered. By estimates of the order of magnitudes of terms in the governing equations, a parameter range map is derived. This contains 14 entries, each of which signifies a particular set of qualitative properties of the solidification process. In each case, quantitative estimates for solidification time, degree of undercooling and segregation, are given. The qualitative and quantitative estimates are confirmed and illustrated by time-dependent numerical simulation of a few typical solidification histories. © 1997 Elsevier Science Ltd. All rights reserved.

1. INTRODUCTION

The properties of an alloy are to a large degree determined by liquid flow phenomena during solidification. Thermal convection in the melt determines the heat transfer and thus influences the crystal structure. Also, solutal convection due to enrichment of additives during solidification, may cause an enriched region at the top of the sample, so called macro segregation. As a prototype of cases that arise in industrial casting processes, this paper deals with cooling at a vertical boundary, as indicated in Fig. 1. During solidification, the mold is typically divided into three regions, liquid, solid and mush. The latter is a two-phase region consisting of melt slowly seeping through a forest of solid crystals (dendrites). Other flow phenomena in solidification are reviewed by Huppert [1].

In the last decade, significant progress has been made in the mathematical modelling of binary solidification. Solidification simulations that predict liquid motion, temperature and composition, and thus segregation, are now possible. A far from complete list of such studies is Refs. [2–8]. A few quantitative comparisons with experiments, with varying success, have also been reported [3–8]. However, simulated results are usually presented in dimensional units for particular systems and it is difficult to draw any general conclusions that would apply to other systems.

A well known qualitative feature of different modes of freezing in casting processes is the 'freezing range" [9]. For an alloy of short freezing range, the mushy zone is narrow compared to the width of the casting. This type of freezing occurs in practice in casting of for example pure metals, low carbon steels and commercial copper, aluminum, zinc and tin. The long freezing range is characterised by the absence of distinct solid and liquid regions. The mush fills the entire mold and crystals form and grow throughout the casting. Examples of alloys that solidify in this manner

are aluminum alloys, magnesium alloys, tin bronzes and red brass. There are also examples of intermediate behavior. In such cases the freezing process is "quite sensitive to the rate of freezing" [9], indicating that the freezing range is not determined by the material properties alone, but also by the solidification process.

Since there are a number of different phenomena at play during solidification, even a qualitative understanding is difficult. Scaling analysis has been used to discuss various solidification problems without a mush [10–12]. The instabilities leading to chimney formation in a mush growing from a horizontal surface are discussed using scaling arguments and non-dimensional formulations [13–15]. The scaling analysis of free convection of a simple liquid in enclosures is well known [16, 17]. However, the scaling laws and the different parameter ranges of the complete freezing process for alloys solidifying from a vertical boundary has received very little attention in the past.

An experienced material scientist can often tell whether a particular solidification experiment will show large or small macrosegregation, dendritic or equiaxed crystal structure etc. Scaling laws are not established however, and it is thus difficult to extrapolate results to processes that are less well known.

It is the purpose of this paper to attempt a scale analysis of binary solidification problems, taking into account the most important flow, heat and mass transfer phenomena. The study is restricted to low Prandtl number liquids, with prescribed heat flux cooling at vertical walls. The main result is a table identifying qualitatively different parameter ranges. Representative cases are simulated numerically in order to test the qualitative and quantitative predictions.

2. FORMULATION

A two-dimensional, rectangular mold initially filled with a melt of uniform temperature T_i and com-

NOMENCLATURE

$A = H/B$ aspect ratio

B width of container [m]

$Bo = \alpha g \Delta T_s \cdot H^4/\kappa^2$ liquid region Boussinesq number

$Bo_c = \beta g c_i(1/k_p - 1) \cdot H^3/D^2$ solutal Boussinesq number in liquid region

C specific heat [J kg^{-1} K^{-1}]

c concentration [dimensional]

D mass diffusivity [m^2 s^{-1}]

$Da = \sqrt{G_r}/B$ Darcy number

G_r reference permeability [m^2]

H height of container [m]

k thermal conductivity in liquid [W m^{-1} K^{-1}]

k_p partition ratio, c_s/c_l in mush

L latent heat of fusion [J kg^{-1}]

$Le = \kappa/D$ Lewis number

$p = p'/(\rho_0\kappa^2/B^2)$ pressure (p' is dimensional)

$Pr = \nu/\kappa$ Prandtl number

q prescribed heat flux at cooled wall

$Ra_m = (\beta/\Gamma - \alpha)gBG_r\Delta T_m/(\kappa\nu)$ mush Rayleigh number

$St = Lk/(CqB)$ Stefan number

$St_m = L/C\Delta T_m$ mush Stefan number ($\Delta T_m = \Gamma c_i(1/k_p - 1)$)

$St_s = L/(C\Delta T_s)$ superheat Stefan number ($\Delta T_s = T_i - T_L(c_i)$)

$t = t'/(B^2/\kappa)$ nondimensional time (t' is dimensional)

T temperature [K]

$T_L(c_l) = T_0 - \Gamma c_l$ liqiudus temperature

$\mathbf{u} = \mathbf{u}'/(\kappa/B)$ velocity vector

$\mathbf{x} = \mathbf{x}'/B$ position vector (nondimensional).

Greek symbols

α thermal expansion coefficient

β solutal expansion coefficeint

Γ slope of liquidus line [K (wt frac)$^{-1}$]

δ nondimensinal estimate of mush width

$\eta = (c - c_i)(k_p/c_i(1 - k_p))$ nondimensional concentration

$\theta = (T - T_L(c_i))(k/qB)$ nondimensional temperature

κ thermal diffusivity [m^2 s^{-1}]

ν kinematic viscosity [m^2 s^{-1}]

ρ density [kg m^{-3}]

ϕ local solid volume faction.

Subscripts

c   numbers characterising solutal convection in the melt

cc   cessation of convection

cs   complete solidification

i   initial values

l   liquid phase quantity

m   mush or mixture quantity

r   reference quantity

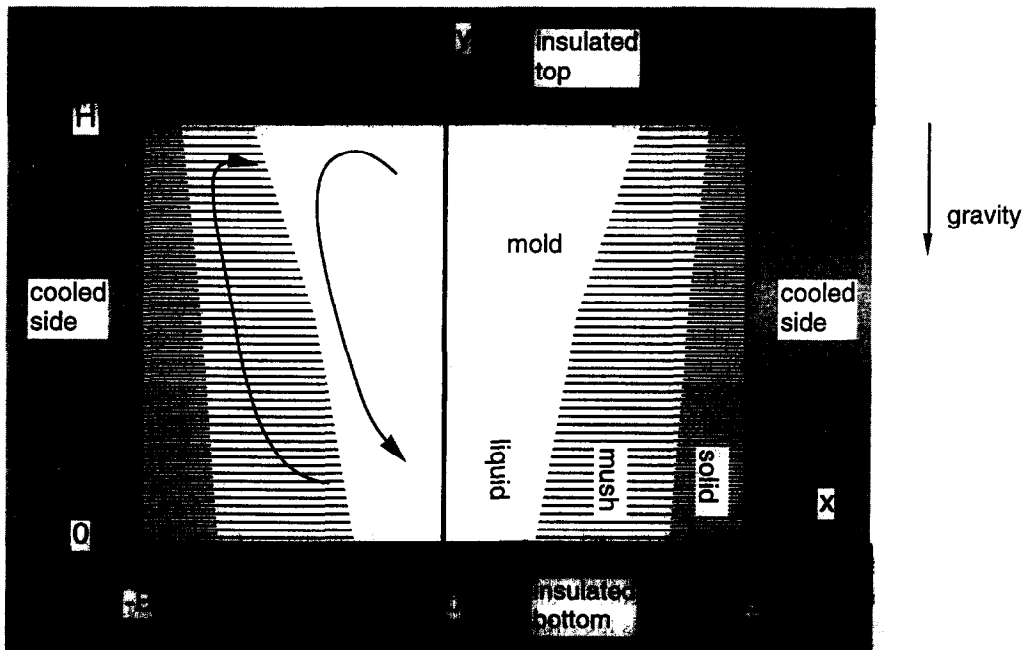s   solid-phase quantity, or number characterising superheat.

Fig. 1. Sketch of the geometry.

position c_i is considered, see Fig. 1. Top and bottom are insulated and a constant heat flux q (Wm^{-2}) is prescribed at vertical sides. This is rather restrictive but can be approximately realised if the major temperature drop from melt to surroundings is over the crucible wall. It has been adopted for simplicity and in order to focus attention on basic solidification.

The process is governed by the fundamental conservation laws and thermodynamical relations describing equilibrium phase change [18]. The standard Boussinesq approximation is invoked, which also implies that solidification shrinkage is neglected. The conservation of linear momentum, mass, heat and solute can be written in the following form, appropriate in the mush $(0 < \phi < 1)$ and the solid $(\phi = 1, \mathbf{u} = 0)$:

$$\frac{Da^2}{Pr}\left(\frac{\partial \mathbf{u}}{\partial t} + \mathbf{u}\cdot\nabla\mathbf{u}\right) - Da^2\nabla^2\mathbf{u} = -\frac{Da^2}{Pr}\nabla p$$

$$-\mathbf{e}_y \cdot Ra_m \cdot \eta_1 - \frac{G_r}{G(\phi)}\mathbf{u} \quad (1)$$

$$\nabla\cdot((1-\phi)\mathbf{u}) = 0 \quad (2)$$

$$\frac{\partial \theta}{\partial t} + (1-\phi)\mathbf{u}\cdot\nabla\theta = \nabla\cdot(k_m/k)\nabla\theta + St\frac{\partial \phi}{\partial t} \quad (3)$$

$$\frac{\partial \eta_m}{\partial t} + \nabla\cdot(\mathbf{u}(1-\phi)\eta_1) = \frac{1}{Le}\nabla^2\eta_1. \quad (4)$$

Here $\mathbf{u} = (u, v)$ denotes the nondimensional fluid velocity, averaged over the pore spaces. p is pressure, θ temperature, η_1 normalised weight fraction of solute in the melt, ϕ local solid volume fraction. $k_m = (1-\phi)k + \phi k_s$ is the mixture thermal conductivity $(k, k_s$ are liquid and solid thermal conductivities). The permeability function $G(\phi)$ multiplying the Darcy term in eqn (1) was chosen as:

$$G(\phi) = H_0 h(\phi)/(1-\phi) \quad (5)$$

where $h(\phi)$ is a nondimensional function chosen according to [7, 19], H_0 (m^2) gives the magnitude of the permeability in the mush. This makes the Darcy term dominating in the mush $(0 < \phi < 1)$, and vanishing in the liquid $(\phi = 0)$. G_r is equal to $G(\phi_r)$, with $\phi_r = 0.2$.

Three additional relations are needed to close the system :

$$\eta_m = (1-\phi)\eta_1 + \phi\eta_s \quad (6)$$

$$\theta = -\frac{St}{St_m}\eta_1 \quad (7)$$

$$\eta_s = (\eta_1 - 1)k_p. \quad (8)$$

Equation (6) is the definition of mixture composition η_m (η_s = solid composition). Equation (7) is the liquidus line of the equilibrium phase diagram, stating that the local freezing temperature in the melt decreases linearly with increasing solute concentration. Equation (8) is the solidus line, which implies

that the dimensional solid concentration is less than the liquid concentration by a factor $k_p < 1$. Implicit in this formulation is the commonly used assumption of rapid mass diffusion within a dendrite arm (the 'lever rule') [20].

The precise definitions of the nondimensional variables are given in detail in the Nomenclature table. They are based on the width B, the time for thermal diffusion over half the width of the sample, and qB/k as the typical temperature difference. The typical concentration change is obtained from the phase diagram as $c_i(1/k_p - 1)$, the melt concentration increases during freezing, in the absence of macroscopic solute transport. Where there is a chance for confusion, a prime designates a dimensional variable.

Several nondimensional numbers appear, see definitions in the Nomenclature. Pr, is assumed to be less than unity for liquid metals, $Le = \kappa/D$ is typically $O(10^4)$ or more. St is a Stefan number based on the typical temperature difference qB/k. Ra_m is a Rayleigh number appropriate for convection through the porous mush [13, 15]. St_m is a Stefan number based on the typical temperature difference over the mush, $\Delta T_m = \Gamma c_i(1/k_p - 1)$. The Darcy number Da may be interpreted as a ratio between a characteristic microscopic length, i.e. dendrite dimensions, and the width of the container. This parameter is not independent from those listed previously, but is retained due to its physical interpretation. It is typically quite small, $O(10^{-3})$ or less.

In the liquid region the appropriate nondimensional form of the equations is, using $\phi = 0$, and $\eta_m = \eta_1$:

$$\frac{\partial \mathbf{u}}{\partial t} + \mathbf{u}\cdot\nabla\mathbf{u} = -\nabla p + Pr\nabla^2\mathbf{u}$$

$$-\left(\theta\frac{Bo\cdot St_s}{A^3 St} + \eta_1\frac{Bo_c}{Le^2 A^3}\right)\mathbf{e}_y \quad (9)$$

$$\nabla\cdot\mathbf{u} = 0 \quad (10)$$

$$\frac{\partial \theta}{\partial t} + \mathbf{u}\cdot\nabla\theta = \nabla^2\theta \quad (11)$$

$$\frac{\partial \eta_1}{\partial t} + \nabla\cdot(\mathbf{u}\eta_1) = \frac{1}{Le}\nabla^2\eta_1. \quad (12)$$

Here A is the aspect ratio H/B, which is assumed to be $O(1)$. Bo is a Boussinesq number $(Bo = Pr\cdot Ra)$ based on the initial superheat $\Delta T_s = T_i - T_L(c_i)$. Bo_c is a solutal Boussinesq number based on the typical concentration difference and mass diffusivity. St_s is a Stefan number based on the initial superheat, $\Delta T_s = T_i - T_L(c_i)$.

The nondimensional formulation is complete when the boundary and initial conditions have been listed. These are :

$$y = 0, A: \quad u = v = \frac{\partial \theta}{\partial y} = \frac{\partial \eta_m}{\partial y} = 0 \quad (13)$$

$$x = 0: \quad u\frac{\partial v}{\partial x} = \frac{\partial \theta}{\partial x} = \frac{\partial \eta_m}{\partial x} = 0 \qquad (14)$$

$$x = 1: \quad u = v = \frac{\partial \eta_m}{\partial x} = 0, \quad \frac{\partial \theta}{\partial x} = -1. \quad (15)$$

The initial conditions are:

$$\mathbf{u} = 0, \quad \theta = \frac{St}{St_s}, \quad \eta_1 = 0, \quad \phi = 0 \quad \text{at } t = 0$$

$$(16)$$

3. DERIVATION OF PARAMETER RANGES

In this section we will identify qualitatively different solidification histories, in terms of the numbers A, Bo, Bo_c, Le, Pr, Ra_m, St, St_m, St_s. Due to space limitations the derivations are brief, a more detailed account is given in the report [21], which is available from the author upon request. Solidification is followed from the molten state and the different possibilities are noted in Tables 1 and 2.

Case 1. Excess superheat; no mush formed initially

If the temperature of the cold wall does not fall below the liquidus temperature when cooling starts, the mold remains completely liquid for some time, see categories 1.x in Tables 1 and 2. Using standard estimates [22], this situation can be shown to occur if:

$$Bo^{1/4}\frac{St}{St_s \cdot A} > 1. \qquad (17)$$

This prevails until the specific heat associated with a bulk temperature drops from T_i to $T_L(c_i) + \Delta T_{bl}$ (ΔT_{bl} = boundary layer temperate drop) has been removed:

$$t_{rsh} = \frac{St}{St_s \cdot A}\left(1 - \left(\frac{St}{St_s \cdot A} \cdot Bo^{1/4}\right)^{-4/5}\right). \quad (18)$$

At this time, the characteristic temperature of the bulk liquid is $T_L(c_i) + \Delta T_{bl}$, and the subsequent evolution is considered as starting from t_{rsh} with values for Bo and St_s based on this bulk temperature, i.e.:

$$\tilde{Bo} = (A \cdot Bo \cdot St_s/St)^{4/5} \quad \tilde{St}_s = St/A(A \cdot Bo \cdot St_s/St)^{1/5}.$$

Here it has been assumed that thin boundary layers appear. If this is not true we have a rather unlikely conductive case, summarised as 1.2 in Table 1.

Case 2. Mush appears immediately

If criterion (17) above is not satisfied, or at times greater than t_{rsh}, a mush appears on the cold wall. There are then three different characteristic temperature differences; ΔT_s, qB/K and ΔT_m. $\Delta T_s = T_i - T_L(c_i)$ is typical of the initial temperature variation over the liquid region. $\Delta T_m = T_L(c_i) - T_s(c_i) = \Gamma c_i(1/k_p - 1)$ is characteristic of the temperature difference across a mush zone.

Case 2.1. Low cooling rate and superheat, wide mush

$\Delta T_s < qB/k < \Delta T_m \leftrightarrow St_s > St > St_m$. First we note that the mush width can be estimated easily:

$$\delta_m = St/St_m = \Delta T_m/(qB/k) \sim (\text{width of mush})/B.$$

$$(19)$$

If $St/St_m > 1$, as in this particular range, the interpretation is instead that the mush covers the entire mold, with a solid fraction variation $\sim St_m/St < 1$.

Next we use eqn (3) to estimate the magnitude of different contributions to heat transfer through the mush and solid:

$$\frac{1}{t}\frac{St}{St_m} \qquad Ra_m\frac{St}{St_m} \qquad 1 \qquad \frac{1}{t}St. \qquad (20)$$

$$\quad 1 \qquad\qquad 2 \qquad\quad 3 \qquad 4$$

Terms 1–4 represent specific heat, convection, conduction, and release of latent heat, respectively. Here we have used $\phi \sim \eta_1 \sim O(1)$ (complete solidification), and thus, from eqn (7), $\theta \sim St/St_m$. In the estimation of term 3 the thermal boundary condition at $x = 1$, (14), has been used. In the momentum equation (1), the main balance is between the buoyant and the Darcy terms for small Da, implying that $|\mathbf{u}| \sim Ra_m$ in the mush.

To estimate the time scale t, we assume that term 2 can be neglected since it is multiplied by the mush Rayleigh number Ra_m, which is not large in applications. Term 3 represents the driving force (sidewall cooling) which must be balanced by either term 1 or 4. $1 \sim 3$ gives an estimate of the time for complete solidification as $t_{cs} \sim St/St_m$, valid if $St_m < 1$. This is summarised as case 2.1(a) in Table 1. The opposite possibility, $3 \sim 4$, implies that $t_{cs} \sim St$ and requires that $St_m > 1$, see 2.1(b) in Table 1. Note that the limiting term in the heat budget is the specific heat associated with ΔT_m in 2.1(a) and the latent heat of fusion in 2.1(b).

A metallurgically important property is the existence of an equiaxed zone, where crystals grow in the interior of an undercooled melt. If the bulk liquid has effectively reached the temperature of the edge of the mush, any slight under-cooling will spread into the liquid region, and the formation of an equiaxed zone will be promoted. The time when this happens can be estimated as the time t_{cc} when the flow ceases to have boundary layer character, see Appendix 1. The condition for the appearance of undercooling is now that the liquid region should persist beyond this time, i.e. $t_{cs} > t_{cc}$, where $t_{cc} \sim 1$ according to (A1.3). In case 2.1(a) in Table 1, $t_{cs} \sim St/St_m > 1 \sim t_{cc}$. Similarly for case 2.1(b) $t_{cs} \sim St > St_m > 1 \sim t_{cc}$. Thus a large equiaxed region could appear for both cases.

Another property of interest is macrosegregation, which is estimated in Appendix 2, the results for 2.1(a) and (b) are given in Table 1. These two parameter ranges are the two most favourable for segregation.

Case 2.2. High cooling rate, mush temperature difference greater than superheat, narrow mush

Table 1. Summary of parameter ranges

1.1. *Large initial superheat, no mush initially.*
$Bo^{1/4}St/(A \cdot St_s) > 1 \ (Bo \cdot A \cdot St_s/St)^{1/5} > A.$
no mush forms until $t \geqslant t_{rsh} = St/(A \cdot St_s)(1 - (St/(A \cdot St_s) \cdot Bo^{1/4})^{-4/5})$
At $t \geqslant t_{rsh}$ use range 2 with modified Bo, St_s:
$\quad \tilde{B}o = (A \cdot St_s/St \cdot Bo)^{4/5} \quad \tilde{St}_s = St/A(A \cdot St_s/St \cdot Bo)^{1/5}$

1.2. *Low cooling rate and large superheat, no mush initially.*
$Bo^{1/4}St/(A \cdot St_s) > 1 \ (Bo \cdot A \cdot St_s/St)^{1/5} < A.$
no mush forms until $t \geqslant t_{rsh} = St/St_s$
$\quad$ At $t \geqslant t_{rsh}$ use range 2 with modified Bo, St_s: $\tilde{B}o = St_s/St \cdot Bo \quad \tilde{St}_s = St$

2.1. *Low cooling rate and superheat, wide mush*: $St_s > St > St_m$ $Bo^{1/4}St/(A \cdot St_s) \leqslant 1$	**2.1(a) *Small latent heat, $St_m < 1$.*** solidification time: $\quad t_{cs} \sim St/St_m > 1$ undercooling: $\quad$ undercooling at $t \sim t_{cc}$ estimate of segregation: $\quad a_1(\phi_r, k_p) \cdot Ra_m \cdot St_m/(ASt)$ **2.1(b) *Large latent heat, $St_m > 1$.*** solidification time: $\quad t_{cs} \sim St > 1$ undercooling: $\quad$ undercooling at $t \sim t_{cc}$ estimate of segregation: $\quad a_1(\phi_r, k_p) \cdot Ra_m \cdot St_m^2/(ASt)$
2.2. *High cooling rate, mush temperature difference superheat, narrow mush* $St_s > St_m > St$ $Bo^{1/4} St/(A \cdot St_s) \leqslant 1$ $\Rightarrow \delta_m = St/St_m < 1$	**2.2(a) *Small latent heat, $St < f(St/St_m)$.*** solidification time: $\quad t_{cs} \sim f(St/St_m)/A < 1$ undercooling: $\quad$ no undercooling ($t_{cs} < t_{cc} \sim 1$) estimate of segregation: $\quad a(\phi_r, k_p) \cdot Ra_m(St/St_m)f(St/St_m)/A$ **2.2(b) *Large latent heat, $St > f(St/St_m)$.*** solidification time: $\quad t_{cs} \sim St$ undercooling: $\quad$ undercooling if $St > 1 \ (1 \sim t_{cc})$ estimate of segregation: $\quad a(\phi_r, k_p) \cdot Ra_m St^2/(St_m A)$
2.3. *High cooling rate, superheat > mush temperature difference, narrow mush* $St_m > St_s > St$ $Bo^{1/4}St/(A \cdot St_s) \leqslant 1 \Rightarrow \delta = St/St_m < 1$	**2.3(a) *Small latent heat, $St < f(St/St_s)$.*** solidification time: $\quad t_{cs} \sim f(St/St_s) < 1$ undercooling: $\quad$ no undercooling ($t_{cs} < t_{cc} \sim 1$) estimate of segregation: $\quad a(\phi_r, k_p) \cdot Ra_m(St/St_m) f(St/St_s)/A$ **2.3(b) *Large latent heat, $St > f(St/St_s)$.*** solidification time: $\quad t_{cs} \sim St$ undercooling: $\quad$ undercooling if $St > 1 \ (1 \sim t_{cc})$ estimate of segregation: $\quad a(\phi_r, k_p) \cdot Ra_m St^2/(St_m A)$
2.4. *Very low cooling rate, mush temperature difference > superheat.* $St > St_s > St_m$ $Bo^{1/4}St/(A \cdot St_s) \leqslant 1$ $\Rightarrow Bo < 1$	**2.4(a) *Small latent heat, $St_m < 1$.*** solidification time: $\quad t_{cs} \sim St/St_m > 1$ **2.4(b) *Large latent heat, $St_m > 1$.*** solidification time: $\quad t_{cs} \sim St > 1$
2.5. *Very low cooling rate, superheat > mush temperature difference.* $St > St_m > St_s$ $Bo^{1/4}St/(A \cdot St_s) \leqslant 1$ $\Rightarrow Bo < 1$	**2.5(a) *Small latent heat, $St_s < 1$.*** solidification time: $\quad t_{cs} \sim St/St_s > 1$ **2.5(b) *Large latent heat, $St_s > 1$.*** solidification time: $\quad t_{cs} \sim St > 1$
2.6. *Very low cooling rate and mush temperature difference.* $St_m > St > St_s$ $Bo^{1/4}St/(A \cdot St_s) \leqslant 1$ $\Rightarrow Bo < 1$	**2.6(a) *Small latent heat, $St_s < 1$.*** solidification time: $\quad t_{cs} \sim St/St_s > 1$ **2.6(b) *Large latent heat, $St_s > 1$.*** solidification time: $\quad t_{cs} \sim St > 1$

Here

$$t_{cc} = 0.57 - 4A \cdot Bo^{-1/4}.$$

The segregation estimate $\dfrac{\int (c_m - c_i) \, dA}{(c_{lr} - c_i)2B \cdot H/2}$ is

$$\text{for } St_m < St: \quad a_1(\phi_r, k_p) \frac{Ra_m t}{A} \frac{St_m^2}{St^2}$$

$$\text{for } St < St_m: \quad a_2(\phi_r, k_p) \frac{Ra_m \delta_m t}{A}$$

where

$$a_1(\phi, k_p) = \frac{(1 - (1 - k_p)\phi_r)(1 - \phi_r)}{\phi_r k_p}$$

$$a_2(\phi_r, k_p) = \frac{\phi_r k_p (1 - \phi_r)}{1 - \phi_r(1 - k_p)}.$$

This expression estimates the relative size of segregated volume which has composition

$$\frac{c_i}{1 - \phi_r(1 - k_p)}.$$

Table 2. Qualitative properties of the most important parameter ranges

1.1 $Bo^{1/4} \dfrac{St}{A \cdot St_s} > 1$	Large initial superheat, no mush initially.
2.1 $St_s > St > St_m$ $Bo^{1/4} \dfrac{St}{A \cdot St_s} \leq 1$	A mush of approximately uniform solid fraction covers the mold.
2.2 $St_s > St_m > St$ $Bo^{1/4} \dfrac{St}{A \cdot St_s} \leq 1$	Mush forms a front. Distinct solid, mushy and liquid regions.
2.3 $St_m > St_s > St$ $Bo^{1/4} \dfrac{St}{A \cdot St_s} \leq 1$	Includes the pure metal case.

$\Delta T_s < \Delta T_m < qB/k \leftrightarrow St_s > St_m > St$. This range includes cases with very rapid solidification. The expected mush is narrow, $\delta_m \sim St/St_m < 1$. The main contribution to the heat budget is the specific heat in the mush and solid regions, and convection is less important.

The temperature must decrease by approximately ΔT_m for complete solidification. The time required was estimated from a simple one dimensional heat diffusion problem: If $\theta_i = 0$ at $t = 0$, and a cooling rate $\partial \theta / \partial x = \mp 1$ is maintained at $x = \pm 1$, the temperature at the centreline $x = 0$ is:

$$-\theta = f^{-1}(t)$$

$$= 2 \left(2 \sqrt{\frac{t}{\pi}} e^{-1/4t} + \text{erf}\left(\frac{1}{2\sqrt{t}}\right) - 1 \right). \quad (21)$$

A temperature decrease of ΔT_m corresponds to a change of $- St/St_m$ in θ, so the estimated solidification time is

$$t_{cs} = f(St/St_m).$$

Here the latent heat release has been neglected. If it is instead limiting, the nondimensional time required to remove the latent heat is $t_{cs} = St$. If this is greater than the cooling solidification time $f(St/St_m)$, the latent heat is considered to be limiting, or vice versa, i.e.: if $f(St/St_m) > St$, then $t_{cs} = f(St/St_m)$, else $t_{cs} = St$. These cases are summarised in Table 1 as 2.2(a) and 2.2(b).

In the case of 2.2(a), the time for complete solidification $t_{cs} = f(St/St_m)$ is always less than unity, i.e. $t_{cs} < 1 \sim t_{cc}$ so that no undercooling of the bulk liquid

is possible. The narrow mushy region will always have time to traverse the container before the average temperature of the liquid has approached $T_L(c_i)$. In case 2.2(b) the criterion for undercooling is instead $t_{cs} = St > 1 \sim t_{cc}$.

The segregation estimates for case 2.2(a and b) indicate generally low segregation. If the mushy layer is very narrow however, mass transfer through the mush may be diffusive rather than convective as assumed, and an enriched liquid region may result [11, 12, 21, 23].

Case 2.3. High cooling rate, superheat greater than mush temperature difference, narrow mush $\Delta T_m < \Delta T_s < qB/k \leftrightarrow St_m > St_s > St$. This is a short freezing range case rather similar to 2.2. The only qualitative difference is that ΔT_m is now the smallest temperature difference. This implies that, unlike case 2.2, solidification of a pure substance is included as the limiting case $St_m \to \infty (\Delta T_m \to 0)$.

Cases 2.4–2.6. No convection, Bo < 1. The remaining cases in Table 1, 2.4–2.6, all satisfy $St/St_s > 1$ and $St/St_s \cdot Bo^{1/4} < 1$, which implies that $Bo < 1$. These are thus the rather exotic cases where dimensions are so small etc., that convection is weak. Due to their limited usefulness, only the results for total solidification time are quoted in Table 1.

4. EXAMPLES AND COMPARISON TO SIMULATIONS

In order to test the predictions in Table 1, these were compared to numerical simulations of a few typical cases. Several additional cases have been tested by Amberg [21]. The numerical code that was used has been described elsewhere, [7, 8]. Here it may suffice to say that it solves the equations in Section 2 time dependently in two dimensions. It has been validated by comparisons to experiments [8], and comparisons to known simple cases.

The most important cases in Table 1 are 1.1, 2.1–2.3. The corresponding solidification histories have been sketched qualitatively in Table 2. In case 1.1 the initial superheat is so large (or cooling so slow) that the time to decrease the wall temperature to the liquidus temperature is appreciable. In case 2.1, which is typical of very slow cooling, a mush of approximately uniform solid fraction spans the cavity. During most of the process there are no solid or liquid regions, instead the solid fraction increases uniformly. Cases 2.2 and 2.3 are typical for more rapid cooling. The solid and liquid regions are distinct and are separated by a thin mush advancing across the mold.

As a starting point, the case simulated in Ref. [7], of an iron -1% carbon system is investigated. The values of the nondimensional numbers for this system are:

$$St = 1.806, \quad St_s = 72.24, \quad St_m = 3.354,$$
$$A = 1.00, \quad Bo = 4.033 \cdot 10^5, \quad Ra_m = 2.490,$$
$$Pr = 0.1742, \quad Le = 5741., \quad Bo_c = 1.084 \cdot 10^{15}.$$

As seen here, $Pr < 1$, $Le \gg 1$, and $Bo_c \gg 1$. Note that Bo_c overestimates the importance of solutal convection in the liquid region, since it is based on the composition change across the mush. The flow in the liquid region is normally dominated by thermal convection [24, 7, 8], even if there are situations when solutal stratification and double-diffusive phenomena are important [4, 25–28].

The predictions from Table 1 are listed in Table 3. It is seen that $Bo^{1/4}(St/ASt_s)$ has a value below one, indicating that a mush will quickly form on the cooled wall. The values of St, St_s and St_m above point to case 2.2(b) in Table 1.

The picture obtained from Table 1 is then that a mushy layer will appear on the cold wall more or less immediately after cooling has begun. The liquid region adjacent to the mush is then cooled by thermal convection until all the liquid has approximately reached the temperature of the mush front. The time for this to happen is estimated as $t_{cc} = 0.4127$ in Table 3. In the absence of undercooling, the mush will then rapidly invade the liquid region. With some undercooling at the mush front, the entire liquid region is cooled to a temperature slightly below the liquidus, thus precipitation of free crystals inside the liquid is promoted. Here it will be assumed that the mush occupies the entire cavity at times greater than t_{cc}.

The ratio $\delta_m = St/St_m$ may be interpreted as the (nondimensional) width of the mush, which in a "typical" case 2.2 should be $\delta_m \ll 1$. Conversely, in range 2.1, $\delta_m = St/St_m > 1$, the mush would cover the cavity and have a solid fraction variation of $0(1/\delta_m)$. Here $\delta_m = 0.5386$, which must really be considered as $O(1)$, so that the mushy region is expected to span the entire cavity, and the variation of solid fraction is $O(1)$. Solidification proceeds by a gradual thickening of the mush until (in this case) the latent heat has been removed at $t_{cs} = 1.806$, when solidification is complete. The estimate of final segregation indicates

Table 3

	$Bo^{1/4}\dfrac{St}{ASt_s}$	t_{rsh} removal of super-heat	$B\tilde{o}$	$S\tilde{t}_s$	t_{cc} cessation of convection	$\delta_m = St/St_m$	t_{cs} complete solidification	Segregation
ref case	0.6300	—	—	—	0.4127	0.5386	1.806	0.1841
1.1–> 2.1(b)	6.300	0.1927	92510.	315.0	0.3421	5.386	18.06	13.06
2.2(a)	0.063	—	—	—	0.4127	0.00539	0.0905	0.0001

t'=10 s, t=0.00574

t'=5 min, t=0.172

t'=10 min, t=0.344

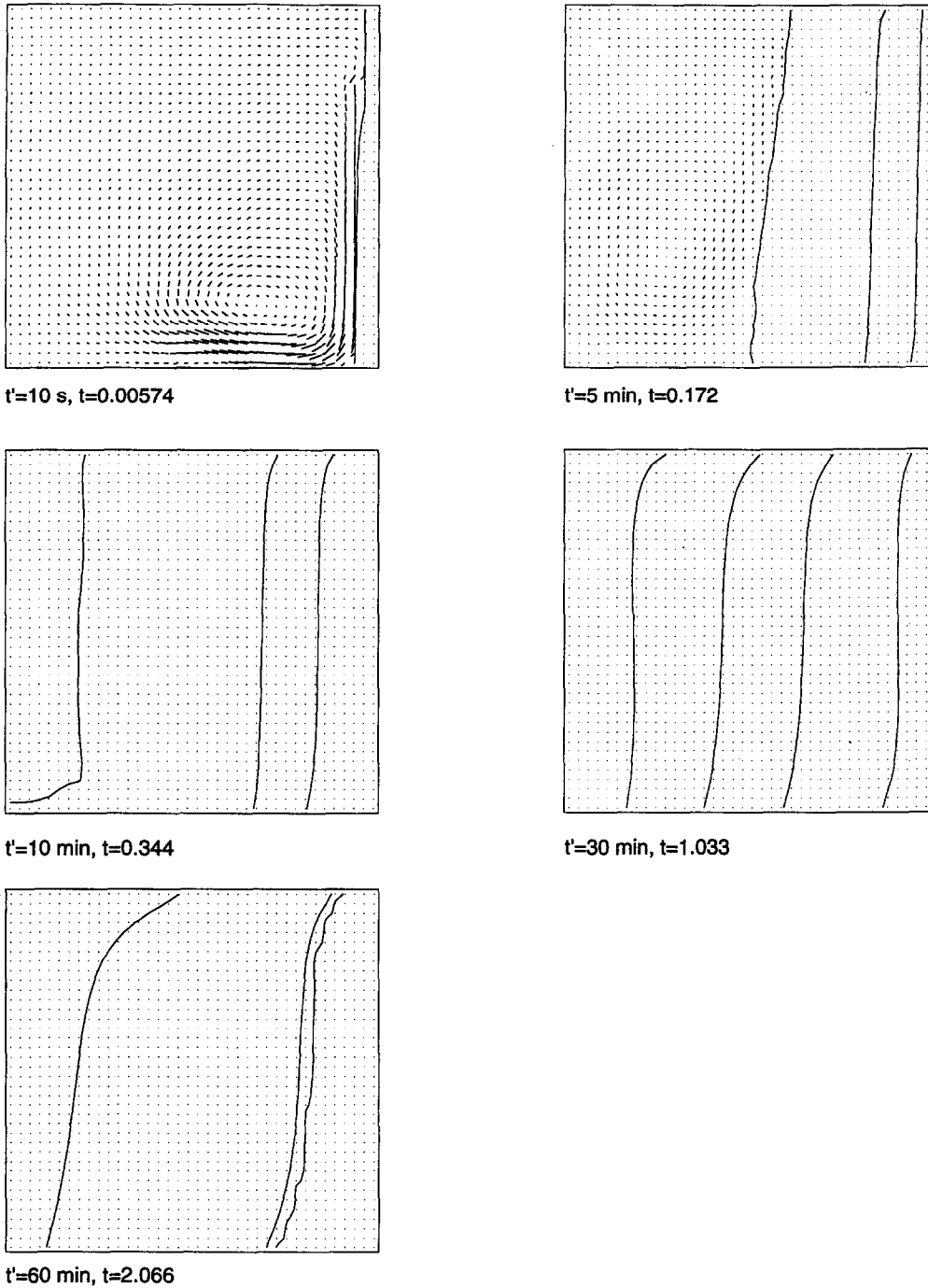t'=30 min, t=1.033

t'=60 min, t=2.066

Fig. 2. Velocity vectors and levels of solid fraction at different times for the reference case (2.2b). the right half of the mold is shown, with cooling from the right (c.f. Fig. 1). The solid fraction levels are 0.001, 0.2, 0.4, 0.6, 0.8, 0.99 and 0.999. An arrow of length equal to the spacing between two mesh points corresponds to a velocity of 1 cm s^{-1}.

a moderate degree of segregation : a little less than 20% of the volume of the sample should have a composition significantly different from the initial one.

Figure 2 shows simulated velocity vectors and solid fraction contours at different times. A mush is seen to grow rather quickly from the cooled wall. The flow in the liquid region in Fig. 2. is a boundary layer free convection type flow at early times, but velocities decrease quickly and the boundary layer thickness increases. After about 8 min 20 s ($t = 0.29$) a thin mush spans the entire cavity. This is in reasonable agreement with the estimated $t_{cc} = 0.4127$.

The further evolution of the mush is also in agreement with the predictions. At $t' = 30$ min ($t = 1.033$) the solid fraction is approximately linear away from the end walls and varies between 0.15 and 0.85, in agreement with the expectation that the mush should have an order one width. The solidification time was obtained as 1 h 12 min. (2.48 nondimensional), which is in reasonable agreement with the order of magnitude estimate 52 min (1.806 nondimensional) obtained above. After solidification perhaps 15% of the area was occupied by enriched and depleted regions, in reasonable agreement with the 18% estimate in Table 3.

Case 1.1 and 2.1b

In order to test the characteristics of the "low cooling rate" range 2.1, a test was made for a case with the same set of dimensional parameters as above, except that the cooling heat flux q was decreased by a factor of 10. This changes St to $St = 18.06$, while all other nondimensional numbers are the same.

The predicted solidification history is illustrated in Fig. 3, the quantitative predictions are listed in Table 3. Now $Bo^{1/4}St/(ASt_s) > 1$ so that the flow is initially described by range 1.1. The time required to remove the excess superheat is estimated to be $t_{rsh} = 0.1927$ (5 min 36 s), when a narrow mush appears. The temperature of the bulk liquid has then decreased, the corrected values $\tilde{Bo}$ and $\tilde{St}_s$ are listed in Table 3. These lead to box 2.1(b) in Table 1, and the remaining entries in the second row of Table 3 are calculated from this. The liquid will now continue to cool towards the temperature of the mush surface. This is expected to be completed after an additional time of $t_{cc} = 0.3421$. As discussed above, the mush is expected to cover the entire mold soon after.

The evolution of the mush is thereafter governed by the ratio $\delta_m = St/St_m$. Here $\delta_m = 5.386 > 1$, which indicates a mush with an $O(1/\delta_m)$ solid fraction variation. We thus expect the subsequent solidification to be a gradual increase in solid fraction, with a variation of solid fraction over the sample less than 0.2. The time for complete solidification is $t_{cs} = St$. Here $t_{cs} = St = 18.1$ is very long compared to the initial phase.

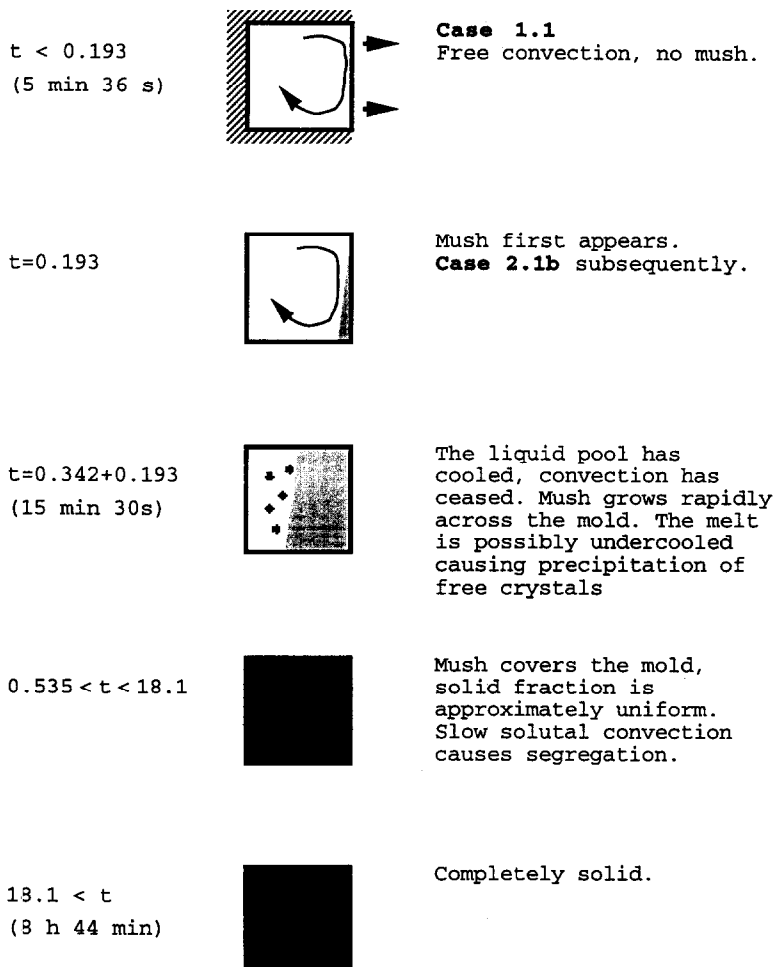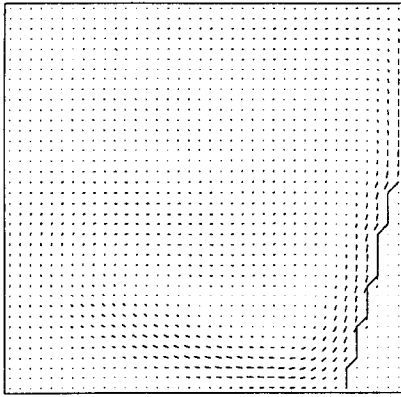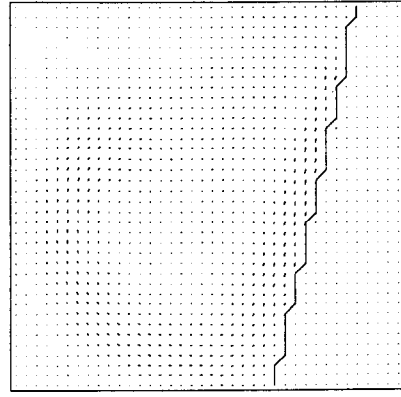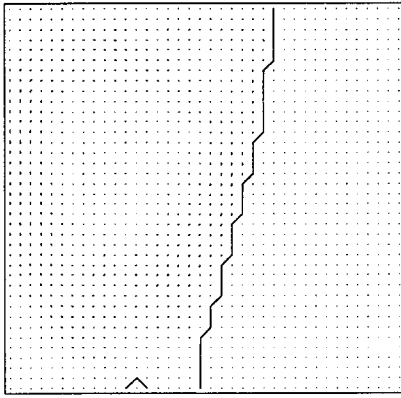Figure 4 shows the simulated velocity vectors and

Fig. 3. Sketch illustrating the predicted solidification history for case 1.1 and subsequent case 2.1(b).
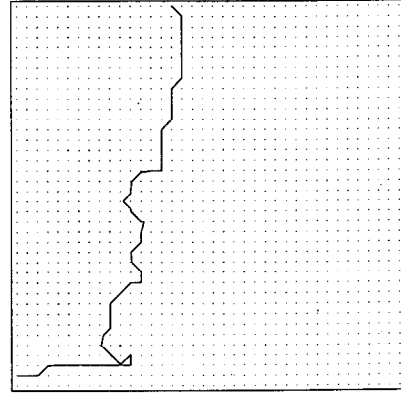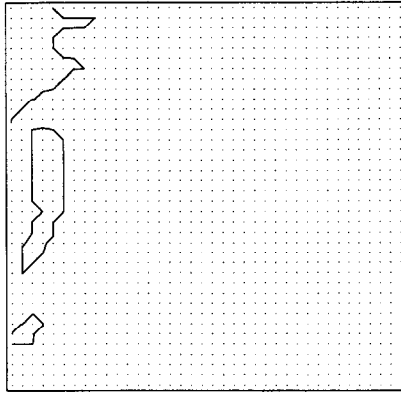
t'=6 min, t=0.2067

t'=9 min, t=0.3100

t'=12 min, t=0.4133

t'=15 min, t=0.5166

t'=18 min, t=0.6200

Fig. 4. Velocity vectors and levels of solid fraction at different times for the 1.1 and subsequent 2.1(b) case. The only solid fraction level that is shown is 0.001, solid fraction is less than 0.2 everywhere. An arrow of length equal to the spacing between two mesh points corresponds to a velocity of 1 cm s^{-1}.

contours of the solid fraction. After 6 min ($t = 0.2067$) a narrow mush has just appeared and covers about half the height of the cooled wall, in good agreement with the estimate $t_{rsh} = 0.193$ in Fig. 3. The mush continues to grow while the convective flow in the liquid becomes weaker, until no flow at all is visible at 15 min ($t = 0.5166$), and the mush fills the cavity at 18 min ($t = 0.62$). This is again in fair agreement with the statement in Fig. 3 that the liquid region should disappear at $t = 0.535$.
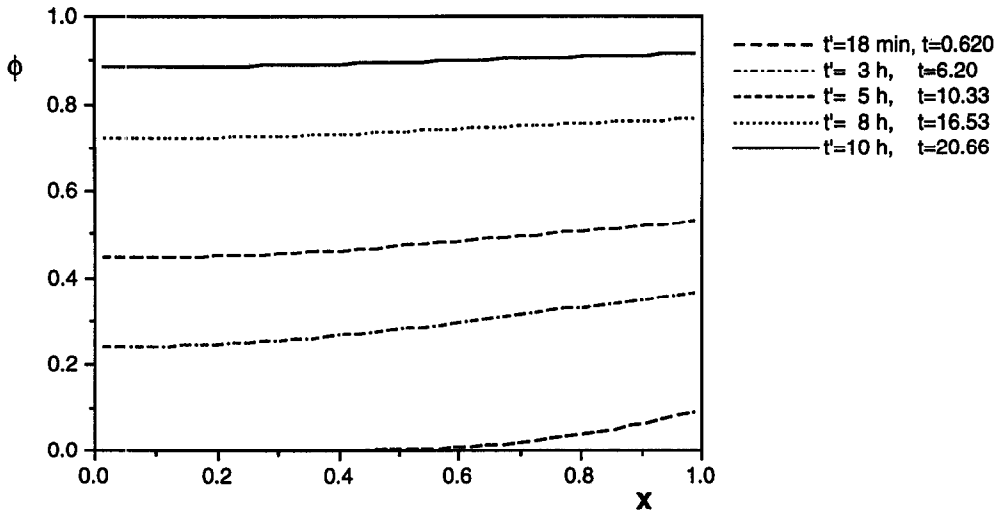
Fig. 5. Solid fraction as a function of x along the mid height $y = A/2$ for the 2.1(b) case, at different times.

The subsequent solidification is shown in Fig. 5, which shows profiles of ϕ vs x at different times, along the mid height $y = 0.5$. The qualitative picture in Fig. 3 of a mush that solidifies uniformly is confirmed. Also the time for complete solidification is found to be 11 h 5 min, or 22.90 nondimensional, in fair agreement with the estimate 8 h 44 min (18.06 nondimensional).

The segregation parameter is 13.06 in Table 3, which should be interpreted to mean that the enriched and depleted regions have merged and that there is no region of initial composition left. The computed final segregation pattern is qualitatively consistent with this picture [21], but shows less segregation than expected. The estimate (A2.2) typically overpredicts segregation, but it is at least able to distinguish between large and small segregation.

Case 2.2(a)

In order to demonstrate a fast cooling range, a value of $q = 6.10^6$ Wm^2 was chosen, with all other dimensional parameters kept as for the reference case. As before, all nondimensional numbers are the same except St which is now decreased to 0.018. This particular choice of q gives unrealistically large temperature differences, but the set of nondimensional numbers are perfectly possible, and this case should be possible to realise with a different alloy. It will thus be discussed mainly in nondimensional terms.

The predictions from Table 1 are given in Table 3. Here $Bo^{1/4}St/ASt_s << 1$, mush appears immediately. The values of the three Stefan numbers St_s, St_m, St lead to cell 2.2(a) in Table 1 and 2, which is a case where the mush is expected to form a narrow front which traverses the mold. The estimated width of this mush is $\delta_m = 0.005 << 1$. The nondimensional solidification time is 0.0905. The time required for the liquid pool to cool is much longer, $t_{cc} = 0.4127$, so

that convection in the liquid region will be vigorous throughout the solidification.

Figure 6 shows velocity vectors and levels of solid fraction. As expected, the transition from solid to liquid is sharp, except for a small region ahead of the front. The significance of this is presently unclear. It may be a numerical artefact, since it is generally not wider than three mesh points.

It is seen in Fig. 6 that the flow in the liquid region has a visible boundary layer character up to time $t = 0.0517$. At $t = 0.0689$, after the width of the liquid region has decreased to approximately the size of two boundary layer thicknesses, the liquid region has been replaced by a thin mush. This supports the conclusion above, that there is not time for the convection in the liquid region to decay before the sample is solidified.

It was found that the mold was completely sold at approximately $t = 0.10$, in good agreement with the predicted $t_{cs} = 0.0905$. The segregation estimate in Table 3 is very small, so there should be virtually no segregation here. This is in agreement with the simulation, where the variation of c_m was within 0.3% of c_i after solidification.

5. CONCLUSIONS

The aim of this paper is to find the different parameter ranges for an alloy solidifying from the side. Several assumptions have been made in the formulation of the basic equations, but still the treatment covers a broad class of binary systems and should be possible to extend easily.

All possible combinations of three typical temperature differences are investigated, and for each one the dominating balance in the heat budget is found. All the different cases are summarised in Table 1, and
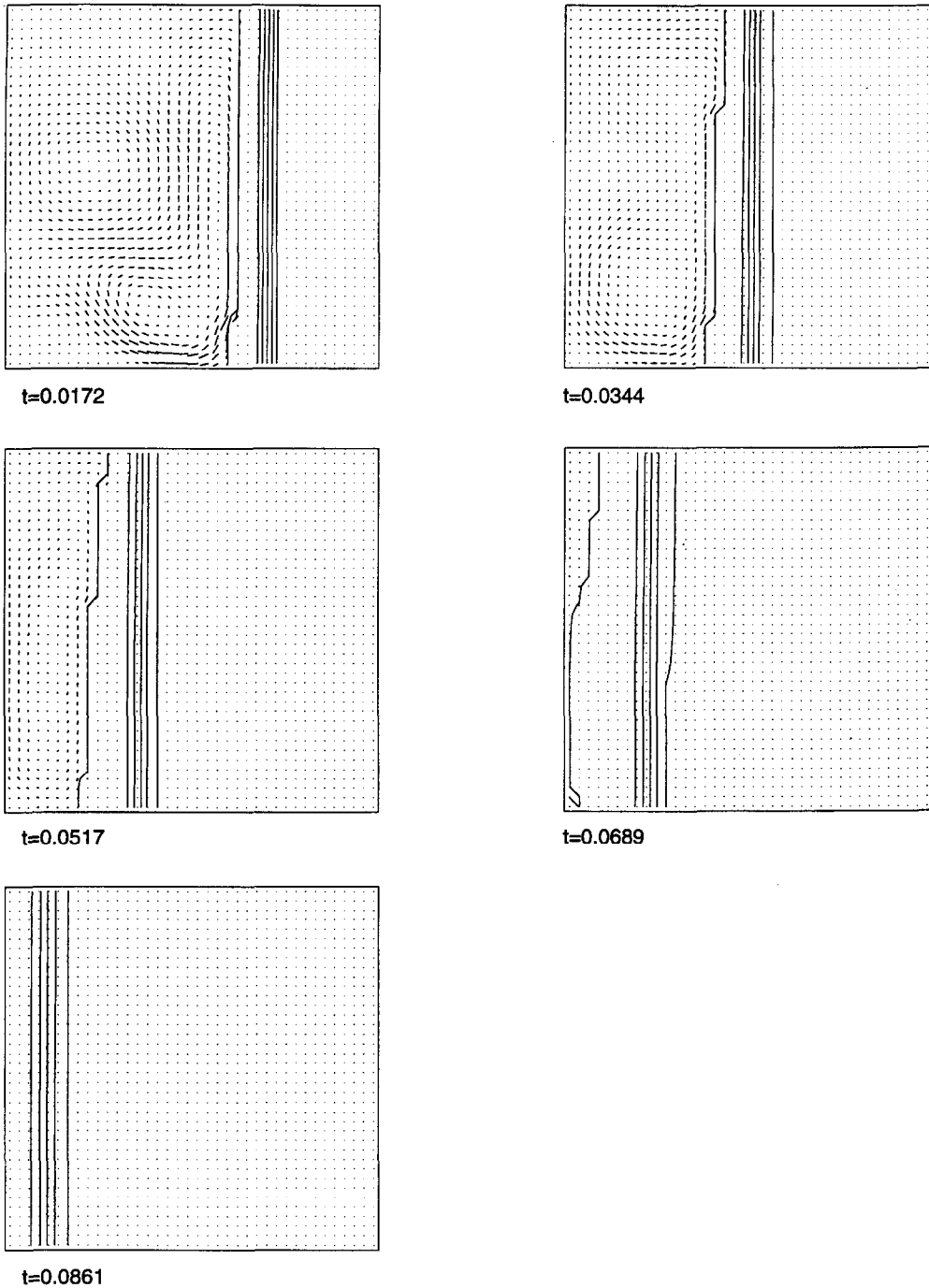
Fig. 6. Velocity vectors and levels of solid fraction at different times for the 2.2(a) case. The solid fraction levels are 0.00001, 0.2, ,0.4, 0.6, 0.8 and 0.999. An arrow of length equal to the spacing between two mesh points corresponds to a velocity of 1 cm s^{-1}.

the qualitative features of the most important ones are sketched in Table 2.

The inequalities in the table involves St, St_s, St_m, Bo, A, Ra_m. This is only six out of the nine independent nondimensional numbers in the nomenclature table. Thus it is concluded that the values of Le, Pr and Bo_c are less significant as long as they satisfy the assumptions $Pr < 1$, $Le \gg 1$, that have been made.

Table 1 covers all possible parameter combinations, so any solidification problem of this type corresponds to one particular cell. For each cell simple estimates for solidification time, the degree of segregation and the mode of freezing have been worked out.

Some of the most important parameter ranges were investigated by time dependent simulation of the solidification process, and the results were compared to

the predictions in Table 1. The qualitative pictures were confirmed. Typically the estimates of times for solidification and undercooling are accurate within 40% of the simulated values. The segregation estimate is less accurate for intermediate segregations, but it can certainly be used to determine if segregation is small or large.

REFERENCES

1. Huppert, H. E., The fluid mechanics of solidification. *Journal of Fluid Mechanics*, 1990, 212, 209–240.
2. Bennon, W. D. and Incropera, F. P., A continuum model for momentum, heat and species transport in binary solid–liquid phase change systems—II. Application to solidification in a rectangular cavity. *International Journal of Heat and Mass Transfer*, 1987, 30, 2171–2187.
3. Christenson, M. S. and Incropera, F. P., Solidification of an aqueous ammonium chloride solution in a rectangular cavity—I. Experimental study. *International Journal of Heat and Mass Transfer*, 1989, 32, 47–68.
4. Christenson, M. S., Bennon, W. D. and Incropera, F. P., Solidification of an aqueous ammonium chloride solution in a rectangular cavity—II. Comparison of predicted and measured results. *International Journal of Heat and Mass Transfer*, 1989, 32, 69–79.
5. Neilson, D. G. and Incropera, F. P., Numerical simulation of solidification in a horizontal cylindrical annulus charged with an aqueous salt solution. *International Journal of Heat and Mass Transfer*, 1990, 33, 367–380.
6. Prakash, C., Two-phase model for binary solid-liquid phase change, part II: some illustrative examples. *Numerical Heat Transfer*, 1990, 18, 147–167.
7. Amberg, G., Computation of macrosegregation in an iron–carbon cast. *International Journal of Heat and Mass Transfer*, 1991, 34, 217–227.
8. Shahani, H., Amberg, G. and Fredriksson, H., On the formation of macrosegregations in unidirectionally solidified Sn–Pb and Pb–Sn alloys. *Metallurgy Transactions A*, 1992, 23A, 2301–2311.
9. Ruddle, R. W., Solidification of castings—general principles of feeding. In *Applied Science in the Casting of Metals*, Ed. K. Strauss. Pergamon Press, 1970, Chap. 13.
10. Szekely, J. and Chhabra, P. S., The effect of natural convection on the shape and movement of the melt–solid interface in the controlled solidification of lead. *Metallurgy Transactions*, 1970, 1, 1195–1203.
11. Thompson, M. E. and Szekely, J., Mathematical and physical modelling of double-diffusive convection of aqueous solutions crystallizing at a vertical wall. *Journal of Fluid Mechanics*, 1988, 187, 409–433.
12. Thompson, M. E. and Szekely, J., Density stratification due to counterbuoyant flow along a vertical crystallization front. *International Journal of Heat and Mass Transfer*, 1989, 32, 1021–1036.
13. Worster, M. G., Instabilities of the liquid and mushy regions during solidification of alloys. *Journal of Fluid Mechanics*, 1992, 237, 649–669.
14. Worster, M. G., Natural convection in a mushy layer. *Journal of Fluid Mechanics*, 1991, 224, 335–359.
15. Amberg, G. and Homsy, G. M., Nonlinear analysis of buoyant convection in binary solidification with application to channel formation. *Journal of Fluid Mechanics*, 1993, 252, 79–98.
16. Patterson, J. and Imberger, J., Unsteady natural convection in a rectangular cavity. *Journal of Fluid Mechanics*, 1980, 100, 65–86.
17. Viskanta, R., Kim, D. M. and Gau, C., Three-dimensional natural convection heat transfer of a liquid metal in a cavity. *International Journal of Heat and Mass Transfer*, 1986, 29, 475–485.
18. Hills, R. N., Loper, D. E. and Roberts, P. H., A thermodynamically consistent model of a mushy zone. *Quarterly Journal of Mechanics and Applied Maths*, 1983, 36, 505.
19. West, R., On the permeability of the two-phase zone during solidification of alloys. *Metallurgy Transactions A*, 1985, 16, 693.
20. Flemings, M. C., *Solidification Processing*. McGraw-Hill, New York, 1974.
21. Amberg, G., Derivation of parameter ranges in binary solidification, TRITA-MEK TR 1993:9. Technical reports from the Royal Inst. of Tech., Dept of Mech., S-100 44 Stockholm, Sweden, 1993.
22. Bejan, A., *Convection Heat Transfer*. Wiley, New York, 1984.
23. Leitch, A. M., Various aqueous solutions crystallizing from the side. In *Structure and Dynamics of Partially Solidified Systems*, Ed. D. E. Loper. Martinus Nijhoff, 1987.
24. Chen, C. F., Briggs, D. G. and Wirtz, R. A., Stability of thermal convection in a salinity gradient due to lateral heating. *International Journal of Heat and Mass Transfer*, 1971, 14, 57–65.
25. Szekely, J. and Jassal, A. S., An experimental and analytical study of the solidification of a binary dendritic system. *Metallurgy Transactions B*, 1978, 9B, 389–398.
26. Turner, J. S. and Gustafson, L. B., Fluid motions and compositional gradients produced by crystallization or melting at vertical boundaries. *Journal of Volcanology and Geothermal Research*, 1981, 11, 93–125.
27. Beckermann, C. and Viskanta, R., Double-diffusive convection during dendritic solidification of a binary mixture. *PhsyicoChemical Hydrodynamics*, 1988, 10, 195–213.
28. Huppert, H. E. and Turner, J. S., Double-diffusive convection. *Journal of Fluid Mechanics*, 1981, 106, 299–329.
29. Leitch, A. M. and Worster, M. G., Laminar free convection in confined regions. *Journal of Fluid Mechanics*, 1985, 156, 301–319.
30. Hyun, J. M., Propagation of the temperature front in heat-up of an initially isothermal fluid. *International Journal of Heat and Mass Transfer*, 1986, 29, 499–501.

APPENDIX 1

Derivation of a simple model for cooling to constant wall temperature

Here a simple model for the evolution of the mean fluid temperature in a container with side walls kept at a constant low temperature is derived. Related, more complete models have been developed in Ref. [29, 30]. Here a much simpler model is derived, which is shown to agree quite well with complete simulations.

For $Bo \gg 1$ the heat transfer is $q = k\Delta T/H \cdot (Bo \cdot \Delta T/\Delta T_s)^{1/4}$ for low Prandtl number fluids [22]. Defining ΔT as the average temperature in the bulk minus the wall temperature, a net heat budget for the liquid is

$$\frac{\partial \Theta}{\partial \tau} = -\Theta^{5/4} \qquad (A1.1)$$

where nondimensional variables $\tau = t\kappa/HB \cdot Bo^{1/4}$, and $\Theta = \Delta T/\Delta T_s$ have been introduced. With the initial condition $\Theta = 1$, the solution is

$$\Theta = \frac{1}{(1+\tau/4)^4}. \qquad (A1.2)$$

The prediction of eqn (A1.2) was compared to a complete numerical simulation, as shown in Fig. A1.1. The agreement is quite sufficient for the present needs.

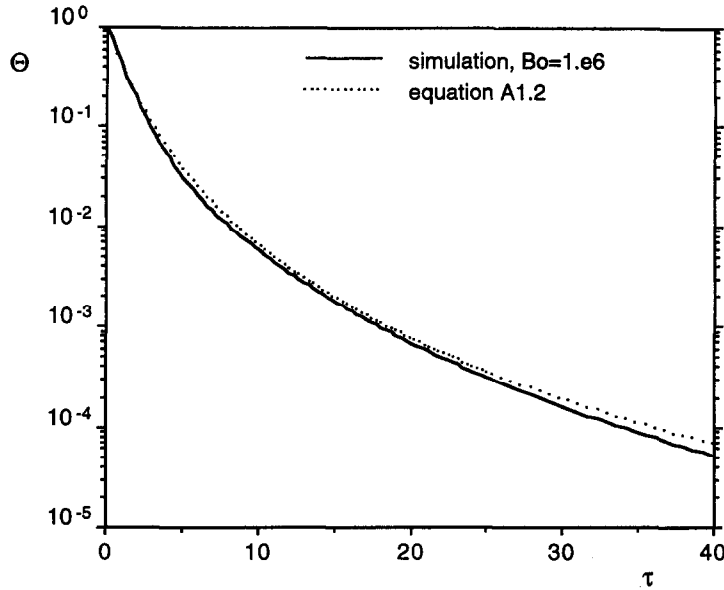This equation is now used to derive an estimate of the time

Fig. A1. Bulk average temperature as a function of time.

when the flow ceases to have boundary layer character. This is assumed to be a sufficient condition of the appearance of undercooling in the liquid region and formation of free equiaxed crystals.

The boundary layer thickness is $\delta \approx 3.53 \cdot H \cdot (\Theta Bo)^{1/4}$. This must be less than half width B of the container, and we take as the criterion for determining the time when convection ceases, that $\delta = B/2$. using eqn (A1.2), and introducing the nondimensional time $t_{cc} = A \cdot Bo^{-1/4}\tau$ we get

$$t_{cc} = 0.57 - 4 A \cdot Bo^{-1/4}. \tag{A1.3}$$

APPENDIX 2

Estimate of magnitude of segregations
Here a crude estimate of the macrosegregation is derived. For a moderate segregation it is expected that enriched (depleted) liquid rises through the mush and forms an enriched (depleted) region at the top (bottom).

For the narrow mush case, $St/St_m < 1$, the composition variation across the mush is $c_i(1/k_p - 1)$. Force balance between the Darcy term and the buoyant term gives $v \sim Ra_m\eta_1$. The total (dimensional) vertical transfer of alloying element during time t is then $(c_{lr} - c_i)(1 - \phi_r)v \cdot B\delta_m \cdot t$, where $c_{lr} = c_i/(1 - \phi_r(1 - k_p))$, and $\phi_r = 0.2$. As a nondimensional measure of the degree of macrosegregation we will now use the ratio of an estimated size of the enriched

area with composition c_{lr}, to the area of the upper half of the sample cross-section :

$$\frac{(c_{lr} - c_i)(1 - \phi_r)v \cdot B\delta_m \cdot t}{(c_{lr} - c_i) \cdot 2B \cdot H/2} = a_2(\phi_r, k_p)\frac{Ra_m\delta_m t}{A}$$

$$\text{(for } St/St_m < 1)$$

where

$$a_2(\phi_r, k_p) = \frac{\phi_r k_p(1 - \phi_r)}{1 - \phi_r(1 - k_p)}. \tag{A2.1}$$

Here δ_m and t denote the nondimensional mush width and time, which are different in different parameter ranges.

In the wide mush case, $St/St_m > 1$, the corresponding estimate becomes (using $\eta \sim St_m/St$) :

$$\frac{\int(c_m - c_i)\mathrm{d}A}{(c_{lr} - c_i)2B \cdot H/2} = a_1(\phi_r, k_p)\frac{Ra_m t St_m^2}{ASt^2}\text{(for } St/St_m > 1)$$

$$\tag{A2.2}$$

where

$$a_1(\phi_r, k_p) = \frac{(1 - (1 - k_p)\phi_r)(1 - \phi_r)}{\phi_r k_p}.$$

If the segregation estimate is less than one, it should be interpreted as the fraction of the cross-section covered by enriched and depleted regions. In the opposite case, all the liquid in the sample has passed through the mush more than once, and the composition is changed over the entire mold.